Int. J. Microgravity Sci. Appl., **35** (4) (2018) 350403
DOI: 10.15011//jasma.35.350403

IIII Original Paper IIII

Effects of Container Materials on X-ray Fluorescence Spectra and Detection Time for *In-situ* X-ray Fluorescence Composition Analysis of Liquid Metals

Masato SHIINOKI[1], Yuki ANDO[1], Hideto FUKUDA[1], Shinsuke SUZUKI[2] and Tadahiko MASAKI[3]

Abstract

The X-ray fluorescence spectra of a liquid metal were analyzed using an X-ray fluorescence analysis, and the effects of the container materials on the peak intensities of a liquid metal using an X-ray fluorescence analysis were experimentally clarified. The spectrum of a liquid metal ($Sn_{57}Bi_{43}$) at 443 K with a container material (graphite or quartz) was measured using an X-ray fluorescence analysis. As a result of the experiments, sharp peaks of Sn and Bi were observed with each container material, and the Compton scattering peak from the X-ray tube was detected using graphite. In addition, by combining the Lambert-Beer law with the model used in the experiments, a theoretical formula was derived. Because the derived formula agreed well with a determination coefficient of 0.979 or higher, the validity of this formula was confirmed. The variation coefficient, which indicates the reproducibility, of an X-ray fluorescence analysis using the container materials was 2.3% for quartz (thickness of 0.3 mm) and 2.1% for graphite (thickness of 2.0 mm) at a detection time of 180 s. Moreover, to obtain the reproducibility, the detection time should be set to longer than 300 s (graphite) and 480 s (quartz), which are comparable to the times required by inductively coupled plasma-optical emission spectrometry.

Keywords: Liquid metal, X-ray fluorescence analysis, *In-situ* observation, Real-time analysis.

Received 6 August 2018, accepted 22 October 2018, published 31 October 2018.

1. Introduction

An *in-situ* analysis of the composition in liquid metals is strongly desired in the metallic material processes and measurements of the properties in liquid metals [1, 2]. In particular, the thermophysical properties in liquid metals are needed for understanding the metallurgical phenomena. An *in-situ* analysis of the composition in liquid metals is expected to be applied to the space experiments without the collection of samples. For example, an *in-situ* analysis can be adapted to measure the composition of liquid metals without a container, such as a levitation technique, [3, 4] when the thermodynamic properties of the liquid metal, namely, the density, surface tension, and thermal conductivity, are measured. In contrast, there is a possibility of adaptation in measuring the changing composition of liquid metals in a container, for example, in the diffusion process [5, 6]. Two types of *in-situ* measurement methods, an X-ray radioscopy (XRR) analysis and an X-ray fluorescence (XRF) analysis, have already been developed and researched. In the diffusion process, a container must be used in the above methods. However, the effects of the container materials on the *in-situ* measurement methods have not been accurately researched.

Zhang *et al.* measured the composition of Al-Cu system during the entire diffusion time using an XRR analysis, and calculated the interdiffusion coefficient using the long capillary method [7]. The long capillary method is the best-known method applied in diffusion experiments where alloy samples with different compositions are put into the respective halves of a capillary. However, the XRR technique has a limitation in that the compositions of the liquid metals are measured at the same time owing to the use of image shading, which is based on each absorption coefficient [8]. Thus, an XRR analysis can be applied to the measurement of elements with a large difference in the absorption coefficient.

However, an XRF analysis is particularly capable of simultaneously measuring multiple elements with high accuracy. In addition, an XRF apparatus is easier to miniaturize than an XRR apparatus. Therefore, an XRF analysis has recently attracted additional attention, and an adaptation to an XRF analysis with regard to the changing composition of liquid metals such as diffusion using a long capillary method is desired. There are two major advantages of using XRF in diffusion experiments. First, it is possible to measure the concentration distribution of the same sample many times. Second, with the long capillary method, *in-situ* measurements of the composition in liquid metals can eliminate the effects of the change in concentration during the heating and cooling processes. In contrast, the advantage of eliminating the diffusion promotion can also be solved using the shear cell technique [9]. However,

1 Faculty of Science and Engineering, Waseda University, Tokyo 169-8555, Japan.
2 Department of Applied Mechanics and Aerospace Engineering and Kagami Memorial Research Institute of Materials Science and Technology, Waseda University, Tokyo 169-8555, Japan.
3 Department of Materials Science and Engineering, Shibaura Institute of Technology, Tokyo 135-8548, Japan.
(E-mail: stag7211@asagi.waseda.jp)

the shear cell technique has a complicated mechanism compared with the long capillary method. In recent years, Masaki *et al*. developed an *in-situ* method for measuring the composition of alloy components in liquid samples by combining an XRF analysis and the long capillary method [10, 11].

However, an XRF analysis in a high-temperature environment has certain problems regarding the measurement of the liquid metal composition [12]. First, there are limitations in selecting the materials used as a container in a high-temperature environment because it is necessary for the container material to act as a crucible and transmit a large number of X-rays. Second, the minimum time required to analyze a system that continuously changes its concentration through an XRF analysis is unknown. In an XRF analysis, an accurate measurement of the composition of a liquid metal generally requires a long duration. In contrast, the time required for an XRF analysis is limited if a system with continual changes to its concentration is analyzed. Fujita *et al.* also reported the two problems listed above in a diffusion experiment conducted by combining an XRF composition analysis of liquid metals and the long capillary method [11]. Therefore, it is necessary to consider the experimental conditions based on the effects of the container materials for the diffusion experiment with the long capillary method.

In this study, we focus on graphite and quartz as the container materials because they are generally used in crucibles. In addition, they are considered to have a small influence on the analysis because graphite and quartz are composed of light elements. Ujihara *et al.* reported the measurement results of the diffusion coefficients in liquid metals of Ga-Zn through an XRF analysis using a graphite crucible [13, 14]. Shimura *et al.* also reported the measurement results of diffusion coefficients in liquid Ag-Cu metals using an XRF analysis with a graphite crucible [15]. Kanasugi *et al.* analyzed the Zn concentration in aqueous solution of salt (Zinc Chloride) using the combination of an XRF analysis and Mach-Zehnder interferometer using a quartz cell [16]. Based on the experimental results in each experiment, it was possible to use graphite or quartz as a container for an analysis of liquid metals. With the exception of graphite or quartz, Uwabe *et al*. demonstrated *in-situ* measurements of a solute partition coefficient in multicomponent liquid alloys using X-ray transmission imaging, and an XRF analysis using a sapphire container [17]. However, no detailed discussion was made on the conditions of the container materials used.

Therefore, in this research, we aimed at investigating the effects of the container materials on the X-ray fluorescence spectra and the detection time for diffusion experiments of liquid metals through an XRF composition analysis. Considering the effects of the container materials, the conditions for increasing the peak intensities of liquid metals were discussed. The spectrum of liquid metal ($Sn_{57}Bi_{43}$) with a graphite or quartz plate was analyzed with various plate thicknesses and sample-detector gaps. In addition, the theoretical formula was derived through a combination of the Lambert-Beer law with the experiment model. Moreover, the concentration of each diffusion sample with the long capillary method is obtained using an inductivity coupled plasma–optical emission spectrometer (ICP-OES) that has thus far been widely used for sample concentration measurements. On the other hand, in diffusion experiments of liquid metals, the method of analyzing the sample concentration will be necessary to replace the *ex-situ* analysis of ICP-OES by the *in-situ* analysis of XRF in the future. In order to realize the replacement of the method, the conditions of XRF analysis with the container materials are needed with at least the same reproducibility as that of ICP-OES. Therefore, the criteria of the thickness and the detection time for each container material should be clarified to realize the required reproducibility. The coefficient of variation *CV* of an XRF analysis and of an ICP-OES was calculated to evaluate the reproducibility. The reproducibility of XRF analysis with the container materials were discussed with changing the thickness and the detection time.

2. Experimental Procedure

Figure 1 shows schematic diagrams of an energy-dispersive X-ray fluorescence spectrometer and a crucible containing liquid metal. Each device was set at a predetermined position, as shown in **Fig. 1(a)**. An XRF analysis was carried out using a X-ray tube (Mini-X, Ag target, 50 keV, 75 μA, AMPTEK, Inc.) and a detector (X-123SDD, AMPTEK, Inc.). The X-ray apparatus was continuously cooled using a cooling fan for stabilization. The size of the collimator of the Mini-X X-ray tube was ϕ2 mm. Moreover, based on measurements using a fluorescent plate, the relationship between the X-ray beam diameter H [mm] and gap clearance l [mm] in the Mini-X X-ray tube can be expressed as

$$H = 0.117\, l + 3.27 \tag{1}$$

Pure Sn (99.999 at%) and pure Bi (99.999 at%) grains (Kojundo Chemical Laboratory Co., Ltd) were used as samples. The liquid metal of a eutectic alloy $Sn_{57}Bi_{43}$ with a melting point of 412 K was prepared according to the following procedure. Each pure metal was weighted, put into a graphite crucible, shown in **Fig. 1(b)**, and heated at 443 K. To prevent the formation of an air layer between the container material and liquid metal, and to keep the height of the container material constant, a pressurizing function in which the covering plate was pressed with an aluminum pin and an aluminum holder using graphite felt was established (see **Fig. 1(b)**). The size of the covering plate was ϕ41 mm. Based on Eq. (1), the maximum

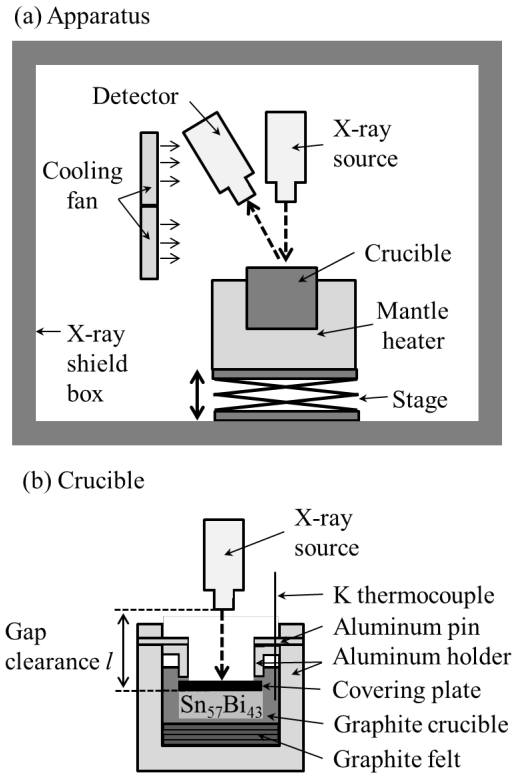

Fig. 1 Schematic diagrams of energy dispersive X-ray fluorescence spectrometer: (a) the entire apparatus and (b) a detailed view of a crucible.

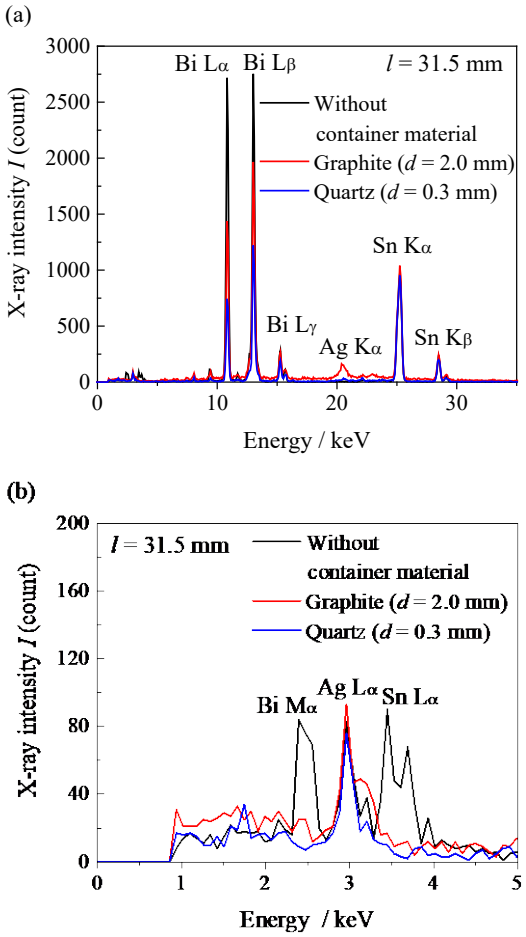

Fig. 2 X-ray fluorescence spectra from liquid $Sn_{57}Bi_{43}$ transmitted through the graphite (d = 2.0 mm), quartz (d = 0.3 mm), and without a container material, where the detection time was 180 s: range of (a) 0 to 35 keV and (b) 0 to 5 keV.

H was 12.4 mm at a gap clearance l of 51.5 mm. Therefore, the X-ray beam diameter did not exceed the size of the covering plate.

The liquid sample was heated constantly to 443 K in an air atmosphere using a mantle heater. A graphite plate, IG-11 (Toyo Tanso Co., Ltd.) with a thickness d of 0.3, 1.0, 1.5, and 2.0 mm, and a quartz glass plate, ESL-2 (Tosoh Corporation), with a thickness d of 0.3 mm, were used for the container materials. The distance between the tip of the X-ray tube and the X-ray tube itself is defined as the gap clearance l and was varied from 31.5 to 51.5 mm by adjusting the stage. The spectrums of $Sn_{57}Bi_{43}$ were acquired using graphite and quartz and without the container materials after each distance was set. The number of measurements n was 10 for each distance.

The CV of the XRF analysis was calculated from the peak intensity of Bi Lβ when the distance l was 31.5 mm. The CV was calculated as follows:

$$CV(\%) = \frac{1}{\bar{I}}\sqrt{\frac{\sum_{i=1}^{n}(I_i-\bar{I})^2}{n-1}} \times 100 \quad (2)$$

Here, $\bar{I}$ is the average intensity, I_i is the intensity obtained in the i-th measurement, and n is the number of measurements.

The CV of the ICP-OES (Agilent 5100, Agilent Technologies, Inc.) was calculated as a standard value to evaluate the reproducibility of the XRF analysis. The eutectic alloy $Sn_{57}Bi_{43}$ used was the same sample as that used in the XRF analysis. The samples were dissolved in a mixture solution of hydrochloric and nitric acids such that the Bi concentration in the solution should be within the range of between 2 and 15 ppm. The measured concentrations were generally the same condition as the dilution with ICP-OES. These samples were analyzed using ICP-OES, and the number of measurements n was 10 for each concentration. The CV was calculated using

$$CV(\%) = \frac{1}{\bar{I}_{ICP}}\sqrt{\frac{\sum_{i=1}^{n}\left(I_{ICP_i}-\bar{I}_{ICP}\right)^2}{n-1}} \times 100 \quad (3)$$

Here, $\bar{I}_{ICP}$ is the average Bi concentration, and I_{ICP} is the value obtained in the i-th measurement of each Bi concentration.

3. Results

3.1 Spectra Peak of SnBi

Figure 2 shows the spectra acquired with graphite (d = 2.0 mm) and quartz (d = 0.3 mm) plates, and without a container material, for a detection time of 180 s and at l = 31.5 mm. As shown in **Fig. 2**, the peaks were observed at the same energy regardless of the container material used. The peak intensities of Sn Kα and Sn Kβ overlapped between the conditions without a container material and with graphite. However, it was confirmed that the X-ray intensity decreases as the energy decreases. In particular, Bi Mα and Sn Lα within the range of 2 to 4 keV were not detectable when the container material was set (see **Fig. 2(b)**). As shown in **Fig. 2**, a peak at around 20.5 keV, which is not a fluorescent X-ray peak of Bi and Sn, was detected. Because the energy peak of 20.5 keV was smaller than that of the fluorescent X-ray, namely, Kα = 22.105 keV[18], for the Ag target of the X-ray tube, it is considered to be a Compton scattering peak of Ag Kα. Therefore, a Compton scattering peak occurs when using the container materials, which is remarkably derived from the X-ray tube.

3.2 Reproducibility of XRF and ICP-OES

Figure 3 shows the *CV* of each XRF analysis. As shown in **Fig. 3**, the *CV* was 1.0–2.5% when using the container material. **Figure 4** shows the *CV* obtained using the ICP-OES. The *CV* of the ICP-OES was less than 1.3% in all concentration ranges. Therefore, it is necessary to obtain the reproducibility of *CV* = 1.3%, which is at least equivalent to ICP-OES. However, the *CV* of each XRF analysis did not reach *CV* = 1.3% with the container material.

4. Discussion

4.1 Effects of container materials on the spectrum

The peak intensity of Sn and Bi was varied based on the container material, and its change increased in order of quartz, graphite, and without a container material. This is thought to be due to the energy dependence of the linear absorption coefficient of the container material. The linear absorption coefficient is described using the Lambert-Beer law, which can be expressed as

$$I = I_0 \exp(-\mu d) \tag{4}$$

$$\mu = \rho \mu_M \tag{5}$$

Here, I is the intensity of the incidence of the X-ray, I_0 is the incident X-ray, d and ρ are the thickness and the density of the substance through which the X-ray is transmitted, respectively, μ is the linear absorption coefficient, μ_M is the mass absorption

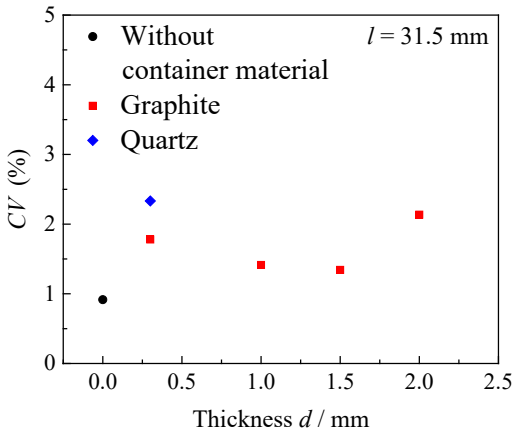

Fig. 3 Coefficient of variation *CV* of the X-ray intensity obtained at l = 31.5 mm, where the detection time was 180 s.

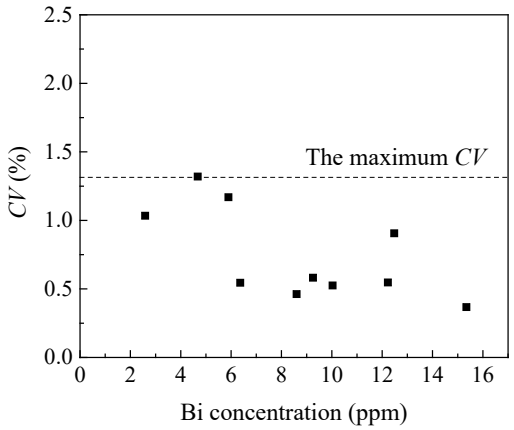

Fig. 4 Coefficient of variation *CV* of the signal intensity obtained using ICP-OES.

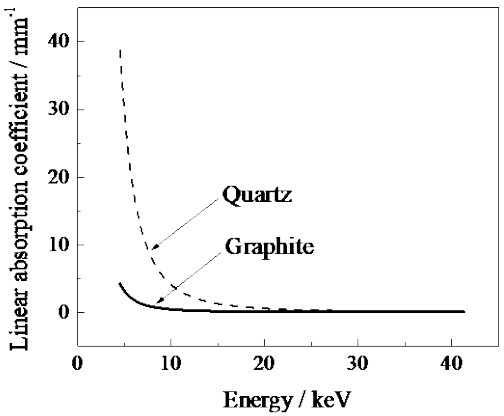

Fig. 5 Linear absorption coefficients of graphite and quartz.

coefficient. The value of μ_M was derived from the literature [19] and was calculated using $E = hc/\lambda$ (h, Planck's constant; c, the speed of light; λ, the wavelength of the photon) from $\lambda = 0.3$ to 2.75 Å with an interval of 0.05 Å. Thus, the linear absorption coefficients of each container material were calculated for Eq. (5).

Figure 5 shows the relationship between energy and the linear absorption coefficient of graphite and quartz. As shown in **Fig. 5**, the linear absorption coefficient on the low energy side increases significantly. Therefore, it was found that the effect of the container materials greatly differs depending on the energy level, that is, the peak position. When the energy level is low, the peak intensity obtained is reduced because the linear absorption coefficient on the low energy side is large. However, the linear absorption coefficient of graphite is smaller than that of quartz near an energy level of 10 keV. Thus, graphite is a preferable container material when the composition of liquid alloys having a peak near an energy level of 10 keV is measured. In contrast, when the energy level is high, there is no change in the peak intensity obtained depending on the container material because the linear absorption coefficient on the high energy side is small.

4.2 Relationship Between the Gap Clearance and X-ray Intensity

Figure 6 shows the relationship between the gap clearance l and X-ray intensity of Bi Lα. It should be noted that the X-ray intensity decreases as the plate thickness increases. In addition, the X-ray intensity of quartz was significantly lower than the X-ray intensity of graphite. This may be due to the fact that the linear absorption coefficient of Si, which is the main component of quartz, is larger than that of graphite.

It was found that the relation between the distance and X-ray intensity of each container material is constant. Therefore, an expression for the relation between the X-ray intensity obtained and the distance was derived.

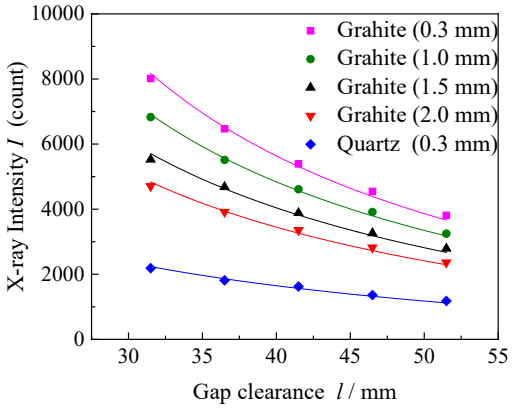

Fig. 6 Relationship between the gap clearance and X-ray intensity of Bi Lα using graphite and quartz plates. Each curve was obtained by fitting Eq. (7). The detection time was 180 s.

Figure 7 shows a model diagram of the experiment. In this model, the intensity of the X-ray fluorescence depends on the distance from the material to the detector, which is expressed as $I = f(1/l^2)$. The gap clearance l includes the thickness of the air layer and the container material layer.

The absorption of X-rays by the substances can be expressed through Eq. (4). When the intensity of the characteristic X-ray I_0 enters the samples, the fluorescent X-ray I emitted from the sample can be written as follows: [20]

$$I = Q\frac{I_0}{\left(\frac{\mu_{\lambda_1}}{\sin\varphi_1}+\frac{\mu_{\lambda_2}}{\sin\varphi_2}\right)\sin\varphi_2} \tag{6}$$

Here, μ_{λ_1} is the mass absorption coefficient of an incident X-ray, μ_{λ_2} is the mass absorption coefficient of a characteristic X-ray, and Q is the emission probability of a fluorescent X-ray.

The symbol I_0 in Eq. (6) includes the effects of the X-ray absorption based on the atmosphere and container material. In Eq. (6), I includes the effects of the X-ray absorption by the atmosphere and the container material, and the X-ray fluorescence depends on the distance from the material to the detector. The intensity of the X-ray fluorescence can be written as follows:

$$I = \frac{K\exp\left[-\sum\rho_n\mu_{n_i}\left(\frac{d}{\sin\varphi_i}\right)-\sum\rho_a\mu_{a_i}\left(\frac{l-d}{\sin\varphi_i}\right)\right]}{\left(\frac{d}{\sin\varphi_1}\right)\left(\frac{\mu_{\lambda_1}}{\sin\varphi_1}+\frac{\mu_{\lambda_2}}{\sin\varphi_2}\right)\sin\varphi_2} \tag{7}$$

Here, ρ_n is the density of a container material, μ_n is the mass absorption coefficient of a container material, ρ_α is the density in the atmosphere, μ_α is the mass absorption coefficient in the atmosphere.

Figure 6 shows the fitted results. To check the theoretical model for changes in the intensity of the X-ray fluorescence, **Fig. 6** was fitted according to Eq. (7) with a fitting parameter of K. The values of K were able to fit between 2.0×10^{11} and 2.5×10^{11} under any conditions. In every container material, the

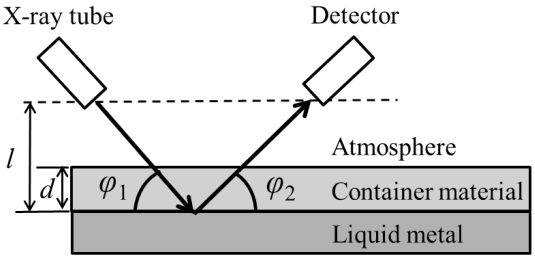

Fig. 7 Schematic diagram of the XRF composition analysis of liquid metal based on the container material.

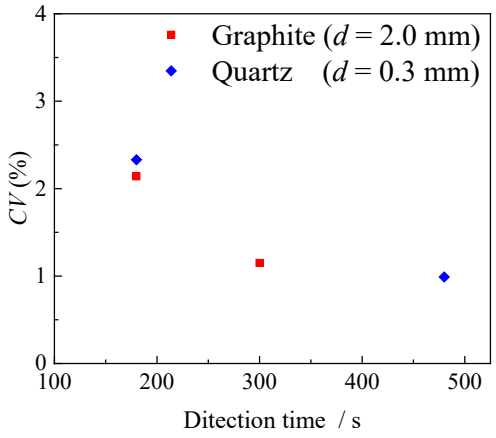

Fig. 8 Relation between the detection time and coefficient of variation *CV*.

coefficient of determination R^2 was greater than 0.979. Because a good fitting result was obtained, the validity of the theoretical formula was confirmed. Therefore, the relationship between the distance and X-ray intensity using the container material can be expressed through Eq. (7).

4.3 Reproducibility

Figure 8 shows the relationship between the detection time and *CV* using graphite (d = 2.0 mm) and quartz (d = 0.3 mm) plates. The *CV* values of the graphite and quartz were 2.1% and 2.3%, respectively, at a detection time of 180 s. The *CV* value can be reduced by extending the detection time. It was possible to improve the coefficient of variation to lower than the maximum *CV* of ICP-OES, namely, 1.3%, as shown in **Fig. 4**, by increasing the detection time, which was 300 s (graphite) and 480 s (quartz), respectively. Therefore, XRF using the container materials can obtain a level of reproducibility equivalent to that of ICP-OES.

4.4 Application for Diffusion Experiments

From the discussion above, the necessary detection time of the diffusion experiments using an XRF analysis was clarified for each container material. It is possible to obtain the accurate intensity sufficient for reproducibility based on the detection time in diffusion experiments using an XRF analysis. In contrast, it is desirable to decrease the detection time for diffusion experiments when applying an XRF analysis because the concentration is continuously changing. Therefore, there are two ways to decrease the detection time.

First, it is suitable to choose a container material that has as small a linear absorption coefficient μ as possible. In particular, graphite is a preferable container material when the composition of liquid alloys having a peak near an energy level of 10 keV is measured. Second, it is suitable to reduce the gap clearance l as close as possible. However, the gap clearance should be sufficiently large to prevent the apparatus from being damaged by heat from the container material.

5. Conclusion

X-ray fluorescence analyses were conducted on liquid metal using graphite and quartz as the container materials. For diffusion experiments of liquid metals using an *in-situ* XRF composition analysis, the detection time should be longer than 300 s (graphite of 2.0 mm) and 480 s (quartz of 0.3 mm) to obtain high accuracy (CV < 1.3%).

In contrast, the detection time should be reduced as much as possible for application of a diffusion experiment of liquid metals using an *in-situ* XRF composition analysis. To reduce the detection time in diffusion experiments while maintaining the reproducibility, the selection of a container material with a small linear absorption coefficient μ, and a reduction of the gap clearance l, is required.

Acknowledgments

This study was supported by the Japan Aerospace Exploration Agency Working group on “Diffusion Phenomena in Melts,” and by a grant-in-aid from Mitsubishi Materials Corporation in the fiscal years 2016 and 2017.

References

1) K. Chiba, A. Ono, M. Saeki and T. Ohno: Bunseki Kagaku, **37** (1988) 365 (in Japanese).
2) T. Ozaki, T. Takahashi, Y. Iwai, K. Gunji and E. Sudo: Tetsu-to-Hagané, **68** (1982) 872 (in Japanese).
3) T. Ishikawa, J.T. Okada, Y. Watanabe, H. Tamaru and Y. Nakamura: Int. J. Microgravity Sci. Appl., **32** (4) (2015) 320410.
4) S. Hakamada, A. Nakamura, M. Watanabe and F. Kargle: Int. J. Microgravity Sci. Appl., **34** (4) (2017) 340403.
5) S. Suzuki, K.-H. Kraatz and G. Frohberg: Ann. N.Y. Acad. Sci., **1027** (2004) 169.
6) S. Suzuki, K.-H. Kraatz and G. Frohberg: J. Jpn. Soc. Microgravity Appl., **22** (3) (2005) 165.
7) B. Zhang, A. Griesche and A. Meyer: Phys. Rev. Lett., **104** (2010) 035902.
8) F. Kargl, M. Engelhardt, F. Yang, H. Weis, P. Schmakat, B. Schillinger, A. Griesche and A. Meyer: J. Phys.: Condens. Matter, **23** (2011) 254201.
9) S. Yoda, H. Oda, T. Oida, T. Masaki, M. Kaneko and K. Higashino: J. Jpn. Soc. Microgravity Appl., **16** (1999) 111. (in Japanese).
10) T. Masaki and S. Suzuki: Space Utiliz, **29** (2015) 103 (in Japanese).
11) K. Fujita, Y. Shimura, S. Suzuki and T. Masaki: Int. J. Microgravity Sci. Appl., **35** (2018) 350404. (in Japanese).
12) T. Ishida, Y. Usui and S. Kinoshiro: JFE Technical Report, **37** (2016) 45 (in Japanese).
13) T. Ujihara, G. Sazaki, S. Miyashita, N. Usami and K. Nakajima: Jpn. J. Appl. Phys., **39** (10) (2000) 5981.
14) T. Ujihara, K. Fujiwara, G. Sazaki, N. Usami and K. Nakajima: J. Cryst. Growth, **241** (2002) 387.

15) Y. Shimura and T. Masaki: Asian Microgravity Symosium, Sapporo, Japan, October 2016, 26SP-A-22.
16) S. Kanasugi, T. Masaki and S. Suzuki: JASMAC 27 abstract, Tokyo, Japan, November 2013, P14.
17) I. Uwabe, K. Dobara, K. Morishita, T. Nagira and H. Yasuda: Tetsu-to-Hagané, **103** (12) (2017) 678.
18) I. Nakai: Keikou X sen Bunseki no Zissai, ed. I. Nakai, 2nd, 259, Asakurashyoten, Tokyo, 2016 (in Japanese).
19) C.H. MacGillavry, G.D. Rieck and K. Lonsdale: International Tables for X-Ray Crystallography: Volume III: Physical and Chemical Tables, Springer, Netherlands, 1983.
20) T. Shiraiwa and N. Fujino: Jpn. J. Appl. Phys., **5** (1966) 886.